PNAS
www.pnas.org

Supplementary Information for

PARL DEFICIENCY IN MOUSE CAUSES COMPLEX III DEFECTS, COENZYME Q DEPLETION, AND LEIGH-LIKE SYNDROME

Marco Spinazzi, Enrico Radaelli, Katrien Horré, Amaia M. Arranz, Natalia V. Gounko, Patrizia Agostinis, Teresa Maia, Francis Impens, Vanessa Alexandra Morais, Guillermo Lopez-Lluch, Lutgarde Serneels, Placido Navas, Bart De Strooper

Corresponding authors: Marco Spinazzi and Bart De Strooper
Email: maspinazzi@gmail.com and bartdestrooper@kuleuven.vib.be

This PDF file includes:

Other supplementary materials for this manuscript include the following:

www.pnas.org/cgi/doi/10.1073/pnas.1811938115

Material and methods

Mice

Mice conditionally targeted and full knockout for *Parl*tm1Bdes (*Parl*$^{lox/lox}$), *Parltm1.1Bdes(Parl*$^{-/-}$*)* were previously generated (1). Nervous system specific *Parl*$^{-/-}$ mice, called *Parl*$^{L/L::}$*Nes*^{Cre}, were generated by crosses with *Tg(Nes-Cre)1Kln* (2) mice that express the recombinase Cre in the central and peripheral nervous system and muscle specific *Parl*$^{-/-}$ mice, called *Parl*$^{L/L::}$*Ckmm*^{Cre}, were generated by crosses with *Tg(Ckmm-Cre)5Khn* (3). Animals are heterozygous for the *Cre* transgene and littermates not having the *Cre* transgene were used as controls. *Pgam5tm1d(EUCOMM)Wtsi* (*Pgam5*$^{-/-}$) full KO mice were obtained after crossing *Pgam5tm1a(EUCOMM)Wtsi* with *Gt(ROSA)26Sortm1*(*Flp1*)*Dym* to obtain conditionally targeted *Pgam5tm1b(EUCOMM)Wtsi* mice which were finally crossed with *Tg(Ella-Cre)C537Lmgd/J*. Mice negative for the *Flp* and *Cre* transgenes were used for further breedings. *Pink1tm1.1Wrst* (*Pink1*$^{-/-}$) mice were kindly provide by Wolfgang Wurst (4). *Ttc19*$^{-/-}$ mice were generated using Crispr/Cas9 technology to target the first exon, encoding the mitochondrial sorting motif. mRNA guides were selected using the CRISPOR web tool (http://crispor.tefor.net/) and tested by a T7 endonuclease assay in mouse embryonic stem cells. Guide 5'-GCAUGUUCCGGUUGCUUCGC-3' was selected. Ribonucleoproteins (RNPs) containing 0.3 µM purified Cas9 protein (Integrated DNA Technologies, IDT) and 0.6 µM CRISPR RNA crRNA and *trans* activating crRNA (IDT) were injected into the pronucleus of C57Bl6J embryos by microinjection in the MutaMouse facility of the KU Leuven. F0 mice were genotyped after weaning using PCR and Sanger sequencing. Founder mice carrying a deletion (D) of 5 nucleotides (D5 +15bp to +19bp, with A of the ATG start codon at position +1) were crossed once with C57Bl/6J and homozygous mice were obtained after breeding heterozygous offspring. The absence of protein or truncated forms was confirmed by western blot analysis using the C-terminal specific Anti-TTC19 antibody

(Sigma HPA052380). Mice were inbred on a C57Bl/6J background and both females and males were included in the study. Mice are housed in cages enriched with wood wool and shavings as bedding, and given access to water and food ad libitum. All experiments were approved by the Ethical Committee on Animal Experimentation of the University of Leuven (KU Leuven).

Pathological analysis

Parl$^{-/-}$ mice and matched WT controls at 2-8 weeks of age were used. Animals were anesthetized with a mixture of xylazine (25 mg/ml), ketamine (20mg/ml) and atropine (20ng/ml), followed by intracardial perfusion of ice-cold phosphate buffered saline (PBS, 10 mL) and ice-cold paraformaldehyde (4% PFA). Head and spine were fixed for additional 48 hrs in 4% PFA at 4 °C. After fixation, brain was removed from the skull and serially sliced using the coronal brain matrix system (Zivic Instruments BSMYS001-1). Five slices were obtained from each brain using the following anatomical landmarks as references: paraflocculi, mammillary body, optic chiasm, olfactory tubercles. Spine was decalcified in a supersaturated solution of tetrasodium EDTA and cross-sectioned at the level of cervical, thoracic and lumbar segments. Samples were embedded in paraffin blocks. Five μm thick sections were stained with hematoxylin and eosin (H&E). Some sections were stained with Luxol Fast Blue, TUNEL or with antibodies against GFAP, IBA1, NEUN, or cleaved CASP3. Microscopic lesions were classified according to the International Harmonization of Nomenclature and Diagnostic Criteria for Lesions in Rats and Mice INHAND criteria (5)

In situ hybridization

In situ hybridization (ISH) was performed as described previously (6). A cDNA-containing construct of *Parl* was generated in the pGemT-easy vector system (Promega). Digoxigenin-labeled antisense and sense RNA probes were generated by in vitro transcription of linearized plasmid using T7 and SP6 RNA polymerase (Roche), respectively. Brains were collected,

fixed with 4% paraformaldehyde overnight, washed with PBS, dehydrated and embedded in paraffin. ISH was performed on 6 µm brain sections using an automated platform (Ventana Discovery, Ventana Medical Systems). Images were obtained by light microscopy and captured with a CH250 CCD camera (Photometrics, Tucson, AZ).

Electron microscopy

Mice of the indicated genotype were transcardially perfused with 2.5% glutaraldehyde, 2% paraformaldehyde in 0.1 M cacodylate buffer pH 7.4 and their brains were post-fixed in the same solution overnight at 4°C. Coronal brain sections (300 µm thick) were cut on a Leica VT1000S vibratome and rectangular pieces of tissue comprising the regions of interest (thalamus, cortex and medulla oblongata) were dissected. The tissue was stored overnight at 4°C in the fixative solution, washed in 0.1 M cacodylate buffer and post-fixed for 2 hours at RT with 1% OsO_4, 1.5% $K_4Fe(CN)_6$ in 0.1 M cacodylate buffer. Sections were rinsed, stained with 3% uranyl acetate for 1 hour at 4°C and dehydrated in graded ethanol concentrations and propyleneoxide, followed by embedding in EMbed812. Resin blocks comprising the brain tissue were sectioned on a Leica Ultracut UCT ultramicrotome (Leica Microsystems). Semithin sections (1 mm) were collected on slides and stained with 1% Toluidine blue solution (Sigma-Aldrich) and mounted in VectaMount mounting medium (Vector). Representative areas were imaged under a Leica DM 2500M light microscope. Ultrathin sections (70 nm) were mounted on copper grids and imaged using a JEM-1400 transmission electron microscope (JEOL), equipped with an 11Mpixel Olympus SIS Quemesa camera. Images were taken at magnifications ranging from 1500X to 15000X.

Subcellular fractionation methods

Mitochondria were purified according to Sims method (7). Brains were rapidly excised, finely chopped with a scissor and homogenized with a Teflon-glass potter in 20 volumes of 20 mM HEPES, 225 mM sucrose, 75 mM mannitol, 1 mM EGTA pH 7.4, on ice. The homogenate

was centrifuged at 900 g for 10 minutes at 4C to remove nuclei and unbroken debris. The supernatant (tissue homogenate) was then centrifuged at 15'000 g for 10 minutes at 4°C. The pellet is the crude brain mitochondrial fraction. The supernatant was spun at 120'000 g for 60 minutes at 4°C to remove particles and the collected supernatant was purified cytosol. The crude brain mitochondrial fraction was re-suspended in 15% Percoll and spun over a discontinuous 24/40% Percoll gradient for 6 minutes at 31,000 g at 4°C. The upper phase containing mainly myelin was discarded. A thick band in the interphase between 15/24% Percoll contains the synaptosomes. Free brain mitochondria were collected at the interphase between 24/40% Percoll. Free brain mitochondria and synaptosomes were washed in isolation buffer to remove residual Percoll.

Cultured cells were pelleted by centrifugation and re-suspended in 10 mM HEPES, sucrose 0,28 M, 1 mM EDTA buffer, pH 7.4 on ice, gently homogenized with a syringe through a 24G needle, followed by a 26G needle, and centrifuged at 800 g for 10 minutes at 4°C. The supernatant was centrifuged at 9000 g for 10 minutes at 4°C. The pellet is the enriched mitochondrial fraction.

To obtain brain nuclear enriched fraction, brain tissue was homogenized in 10 mM HEPES, 1.5 mM $MgCl_2$, 10 mM KCl, 1mM dithiotreitol, pH 7.9 with a Teflon-glass tissue homogenizer on ice. Nuclei and unbroken debris were pelleted by centrifugation at 1000 g for 10 minutes at 4°C. Aliquots of 20 mM HEPES, 0.42 M NaCl, 25% (v/v) glycerol, 1.5 mM $MgCl_2$, 10 mM KCl, 0.2 mM EDTA, 1mM dithiotreitol, pH 7.9 were added to the pellet and mixed by gentle mixing, followed by manual homogenization to facilitate nuclear proteins extraction. The solution was gently mixed for 30 minutes at 4°C, and then centrifuged at 20'000 g for 10 minutes. The supernatant represents the nuclear enriched fraction.

Total tissue and cell culture lysates were obtained by lysis in radioimmunoprecipitation assay (RIPA) buffer on ice and 5 passages with a 26G syringe, followed by centrifugation at 20,000 g for 10 minutes at 4°C to remove unbroken debris.

Immunoblot analysis

Samples were separated in reducing and denaturing conditions in NuPage gels (Invitrogen). Proteins were transferred to PVDF 0.45µm membranes, blocked with milk 5%TRIS-buffered saline, Tween 20 0,1% (TTBS), and incubated with the indicated primary antibodies, washed in TTBS incubated for 1 hour at room temperature with horseradish peroxidase conjugated secondary antibodies (Biorad) in 5% milk-TTBS, and washed in TTBS. Chemiluminescence kit Renaissance (Perkin Elmer) and an Image Quant LAS 4000 mini were used to visualize the proteins.

Blue native gel electrophoresis

Blue-native-gel electrophoresis of digitonin-solubilized mitochondria was performed as described (8). 100 µg isolated mitochondria were solubilized with 600 µg digitonin in Invitrogen Native Page sample buffer on ice for 20 minutes, then centrifuged at 20,000 g for 20 minutes at 4 C. 0,75% Coomassie G-250 was added to supernatants, which were loaded on a 3-12% gradient Invitrogen Native Page gel according to the instructions. After electrophoresis, mitochondrial complexes and super complexes were either visualized by protein staining with Expedeon Instant Blue or immunoblotted on a PVDF membrane and probed with the indicated antibodies.

High-resolution respirometry

Brain mitochondria respiration was measured in Miro6 Buffer (9) (20 mM HEPES, 110 mM sucrose, 10 mM KH_2PO_4, 20 mM taurine, 60 mM lactobionic acid, 3 mM MgCl2, 0.5 EGTA, pH 7.1, 1 mg/ml fatty acid free BSA, catalase 280 U/ml) at 37 °C. When needed H_20_2 was added to reoxygenate the chambers by catalase mediated O_2 generation. 20 µg of purified free

brain mitochondria or 50 µg synaptosomes were loaded into the Oroboros 2K oxygraph. A typical experiment is illustrated in Fig. 4*B*. Oxygen consumption rates were measured before and after addition of the following sequence of substrates and specific inhibitors: 1) 2.5 mM pyruvate, 10 mM glutamate, and 1 mM malate to measure Complex I-driven leak respiration (CI leak); 2) 2.5 mM ADP to determine complex I-driven phosphorylating respiration (CI OXPHOS). When using synaptosomes, digitonin was titrated up to 15 µg/ml to achieve synaptosomal permeabilization resulting in maximal substrate accessibility to neuronal mitochondria and maximal CI OXPHOS; 3) 5 mM succinate to determine the phosphorylating respiration driven by simultaneous activation of complex I and II (CI+II OXPHOS); 4) Titrating concentrations of the mitochondrial uncoupler CCCP to reach the maximal uncoupled respiration (CI+II electron transfer capacity, ET); 5) 200 nM rotenone to fully inhibit complex I-driven respiration and measure complex II-driven uncoupled respiration (CII electron transfer capacity, CII ET); 6) 0.5 µM Antimycin A to block mitochondrial respiration at the level of complex III. Residual oxygen consumption was always negligible. 7); 2 mM ascorbate, 0.5 mM TMPD to measure cytochrome c oxidase (CIV)-driven respiration; 8) 125 µg/ml cytochrome c to evaluate mitochondrial outer membrane integrity 9) 500 µM potassium cyanide (KCN) to specifically block cytochrome c oxidase activity and measure residual background oxygen consumption caused by chemical reaction between ascorbate and TMPD. Cytochrome c oxidase- driven respiration was calculated as the cyanide sensitive oxygen consumption.

Mitochondrial respiratory chain enzyme analysis and CoQ determinations

Respiratory chain measurements were performed according to previously described protocols (10, 11). For the brain, freeze-thawed crude brain mitochondrial fractions were resuspended in 20 mM TRIS, EDTA 2 mM, pH 7.4. An aliquot was kept for CII+III activity measurements which rely on the local concentration of CoQ pools, while the rest was sonicated on ice with a

Branson microtip sonicator at power 20%, 5 seconds ON and 20 seconds OFF for three consecutive times. For muscle, respiratory chain activities were measured on muscle homogenates from gastrocnemius skeletal muscles.

Briefly, Complex I (NADH:ubiquinone oxidoreductase) activity was measured by recording the rotenone-sensitive decrease in absorbance due to oxidation of NADH at 340 nm (ε = 6.2 mM^{-1} x cm^{-1}) in potassium phosphate 50 mM, pH 7.5, BSA 3 mg/ml, KCN 300 µM. The reaction was started by addition of 60 µM ubiquinone$_1$.

Complex II (succinate dehydrogenase) activity was measured by following the reduction of 80 µM 2,6-dichlorophenolindophenol at 600 nm (ε = 19.1 mM^{-1} x cm^{-1}) in potassium phosphate 25 mM, pH 7.5, succinate 20 mM, BSA 1 mg/ml, KCN 300 µM. The reaction was started with 50µM decylubiquinone.

Complex III (ubiquinol cytochrome c oxidoreductase) activity was measured by following the Antimycin A-sensitive reduction of 75µM cytochrome c at 550 nm (ε = 18.5 mM^{-1} x cm^{-1}) in potassium phosphate 25 mM, pH 7.5, Tween-20 0.025%, KCN 500 µM, EDTA 100 µM. The reduction reaction was started by addition of 100µM decylubiquinol.

Complex IV (cytochrome c oxidase; EC 1.9.3.1) activity was measured using the oxidation of 60 µM reduced cytochrome c at 550 nm (ε = 18.5 mM^{-1} x cm^{-1}) in potassium phosphate 50 mM, pH 7.0. The reaction was started by addition of the muscle homogenate.

Complex II + III (succinate cytochrome c reductase) activity was measured using the reduction of 50 µM cytochrome c at 550 nm (ε = 18.5 mM^{-1} x cm^{-1}) in 20 mM potassium phosphate, pH 7.5, succinate 10 mM, 300 µM KCN. The reaction was started by the addition of 50 µM cytochrome c.

ATP synthase reverse enzymatic activity (ATP hydrolysis) was measured by recording the oligomycin-sensitive decrease in absorbance due to oxidation of 200 µM NADH at 340 nm (ε

= 6.2 mM^{-1} x cm^{-1}) in 40 mM TRIS pH 8.0, 0.2 mM EGTA, 2 mM phosphoenolpyruvate, 20 mM $MgCl_2$, 1 mg/ml BSA, 3 µM FCCP, 5 µg/ml Antimycin a, 4 U/ml pyruvate kinase, 4 U/ml LDH, 1 mM ATP.

Respiratory chain enzymes were normalized to the activity of the mitochondrial matrix enzyme citrate synthase. This was measured by recording the increase in absorbance at 412 nm (ε = 13.6 mM^{-1} x cm^{-1}) in a mixture containing 100 µM 5,5′-Dithiobis(2-nitrobenzoic acid) DTNB, 300µM Acetyl CoA, in TRIS 100 mM, pH 8.0, 0.1% Triton X-100, and 500 µM oxaloacetic acid. Citrate synthase enzymatic rates were normalized to the protein concentrations of each muscle homogenate.

CoQ content and the ratio of the reduced vs. oxidized forms were measured as described (12).

Reactive oxygen species production rates analysis

Reactive oxygen species (ROS) were measured fluorometrically at 37 C with an Oroboros Fluorescence-Sensor Green (excitation 525 nm) as described with some modifications (13, 14). 150 µg crude brain mitochondria were loaded in a 20 mM HEPES, 125 mM KCl, 15 mM NaCl, 5 mM KH_2PO_4, 2mM $MgCl_2$, 0,05 mM EGTA, 0,5 mg/ml BSA, pH 7,2 with 10 µM Amplex UltraRed, 1 U/ml HRP, 5 U/ml SOD. A typical experiment is illustrated in *SI Appendix*, Fig.S6*A*. H_2O_2 production was initiated by addition of Complex I substrates (2.5 mM pyruvate, 10 mM glutamate, and 2 mM malate) in absence of ADP to measure Complex I-driven ROS production in the leak state (CI leak), followed by addition of the Complex II substrate (5 mM succinate) to measure Complex I+II ROS production in the leak state (CI+II leak), followed by addition of 2.5 mM ADP to measure ROS production driven by simultaneous activation of complex I and II in the phosphorylating state (CI+II OXPHOS). Finally 0.5 µM Antimycin a was added to measure ROS production driven by inhibited Complex III (Aa). The fluorescence signal for each experiment was calibrated using known

amounts of H_20_2. The chemical background was measured before the addition of mitochondria and this was subtracted from H_2O_2 production rates obtained for each respiratory state. H_20_2 production rates were expressed by mg of mitochondrial proteins.

Detection of protein carbonylation

Protein carbonylation was measured on manually homogenized brains and isolated mitochondria using the recommendations reported by Wang (15). To check for specificity of the assay we included positive controls (samples treated with 1 mM H_2O_2 and 1 mM $FeSO_4$ or with 1 mM H_2O_2 and 1 mM $CuSO_4$) and a negative control (the same sample only treated with 2M HCl but not derivatized with DNPH).

Mitochondrial calcium retaining capacity

Mitochondrial calcium maximal capacity was measured by Oroboros 2K-fluorimetry. Fig. 5A illustrates the protocol by showing the fluorimetric trace of a typical experiment. Chambers were filled with experimental buffer 10 mM MOPS, 120 mM KCl, 10 mM NaCl , 0.5 mM $MgCl_2$, 1 mM KH_2PO_4, 1 mM K_2HPO_4, pH 7.2 (16) containing Complex I substrates 10 mM glutamate/2 mM malate at 37 C. Then, the membrane impermeable calcium indicator Calcium Green 5N was added at a concentration of 1 µM. 500 µg purified brain mitochondria generated by Percoll gradients as described above, were loaded into the chambers resulting in a sharp decrease in Calcium Green fluorescence due to mitochondrial calcium uptake. Once a stable baseline has been obtained mitochondria were challenged with consecutive boluses of 1 µM calcium chloride until no further mitochondrial uptake of calcium could be observed and calcium efflux was observed. 2 mM EGTA was finally injected at the end of the experiment. The maximal calcium retaining capacity was calculated by identifying the maximal capacity of calcium normalized to mitochondrial protein content.

Mitochondrial membrane potential

Mitochondrial membrane potential (Δψ) was measured fluorometrically at 37 C with an O2k-Fluorescence LED module equipped with filter sets for safranin (excitation at 495 nm) according to Kurmschnabel with few modifications (17) as illustrated in Fig. 5B. Safranin was added (to a final concentration of 5 µM for Complex I-driven Δψ and of 4 µM for Complex II-driven Δψ) in the Miro6 Buffer above described without catalase, followed by Complex I substrates (10 mM glutamate, 2mM malate) or with the Complex II substrate succinate and inhibition of Complex I by 100 nM rotenone. In these conditions the mitochondrial membrane potential is inversely related to the fluorescence of safranin, which is quenched in the mitochondrial matrix in hyperpolarized mitochondria. The maximal membrane potential was measured as the difference in safranin fluorescence after addition of exactly 150 µg brain mitochondria in absence of ADP corresponding to the leak state, and after addition of 2.5 mM ADP corresponding to the OXPHOS state. In each experiment the fluorescence signal was calibrated with a standard curve obtained by progressive concentrations of Safranin and the signal was then normalized by setting the maximal basal fluorescence as 1.

Antibodies

A PARL carboxy-terminal antibody was generated in house as previously reported (1). The following commercial available antibodies were employed:

Anti-GFAP, Agilent (DAKO Z033401), anti-IBA1 (WAKO 019-19741), anti- RBFOX3 (NEUN) (EMD Millipore MAB377), anti-NDUFS3 (Abcam ab14711), anti-CYCS (CYTOCHROME C) (BD Phamingen 556433), anti-AIF1 (Santa Cruz-13116), anti-TUBA1A (TUBULIN) (Abcam ab72911), anti-CASP3 (Cell Signaling 9662), anti-cleaved CASP3 (Cell signaling 9661), anti-PARP1 (Cell Signaling 9532), anti-ACTB (ACTIN) (Sigma A5441), anti-HSPD1 (HSP60) (BD Biosciences 611562), ant-UQCRFS1 (Abcam ab14746), anti-

COX4I1 (COX4) (Abcam ab14744), anti-SDH (Abcam ab14715), anti-ATP5B (ATP synthase-beta) (Abcam ab14730), anti-TOMM20 (Santa Cruz sc-11415), anti-PINK1 (Cayman 10006283), anti-PGAM5 (Sigma HPA036979), anti-TTC19 (Sigma HPA052380), anti-COQ3 (Santa Cruz sc-376774), anti-COQ4 (Proteintech 16654-1-AP), anti-COQ5 (Proteintech 17453-1-AP), anti-COQ6 (Proteintech 12481-1-AP), anti-COQ7 (Santa Cruz sc-376484), anti-COQ9 (Santa-Cruz sc-365073), anti-PDSS2 (Santa Cruz sc-515137), anti-SQOR (Novus NBP1-84510), anti-GHITM (Proteintech 16296-1-AP), anti-CLPB (Proteintech 15743-1-AP), anti-STARD7 (Proteintech 15689-1-AP), anti-DIABLO (Cell Signaling 15108), anti-HTRA2 (R&D system AF1458), anti-OPA1 (BD Biosciences 612607), anti-DNP (Millipore 90451).

Proteomic sample preparation

Mitochondria isolated from brain of WT and *Parl*$^{-/-}$ mice were lysed in urea buffer (8 M urea; 20 mM HEPES pH 8.0; and phosphatase inhibitors PhosStop from Roche. For each condition, triplicate samples were prepared. Samples were sonicated with a Branson 450 sonicator by 3 pulses of 10 s at an amplitude of 20% and centrifuged for 15 minutes at 16,000 g at room temperature to remove insoluble components. The protein concentration in the supernatants was measured using a Bradford assay (Bio-Rad) and 500 µg total protein was used for further analysis. Proteins were reduced by adding 4.5 mM DTT and incubation for 30 minutes at 55˚C. Alkylation was performed by addition of 10 mM iodoacetamide for 15 minutes in the dark at room temperature. The samples were diluted with 20 mM HEPES pH 8.0 to a urea concentration of 4 M and proteins were digested with 2 µg endoLysC (Wako) (1/250, w/w) for 4 hours at room temperature. All samples were further diluted with 20 mM HEPES pH 8.0 to a final urea concentration of 2 M and proteins were digested with 5 µg trypsin (Promega) (1/100, w/w) overnight at 37 ˚C. Peptides were then purified on a SampliQ SPE C18 cartridge (Agilent) and from each replicate 100 µg vacuum dried peptides were used for strong cation

exchange (SCX) fractionation. To this end, SCX tips were made by stacking 3 discs (1.5 mm diameter) of polystyrene divinylbenzene copolymer with sulfonic acid (EmporeTM, 3M) in a 200 µl pipette tip. First, the SCX tips were rinsed with 100 µl acetonitrile (ACN) by pipetting the solvent in the tip, flicking the tip so the ACN touches the discs, and pushing the solvent through with a syringe. Then, each sample was dissolved in 100 µl loading buffer (1% TFA in water/ACN (95:5, v/v)) and peptides were loaded on the SCX tip. After washing the tip with 50 µl loading buffer, the peptides were fractionated by subsequently pipetting up and down 20 µl of the following fractionation buffers: 100 mM ammonium acetate, 0.5% FA (fraction 1); 175 mM ammonium acetate, 0.5% formic acid (FA) (fraction 2); 375 mM ammonium acetate, 0.5% FA (fraction 3). Remaining peptides were eluted in 2 x 20 µl of elution buffer (5% NH4OH in water/ACN (20:80, v/v)) (fraction 4). To prevent deamidation in this fraction, 2 µl 10% FA was added. Fractionated peptides were dried in a vacuum concentrator.

LC-MS/MS and data analysis

Dried peptides from each fraction were re-dissolved in 20 µl loading solvent A (0.1% TFA in water/ACN (98:2, v/v)) of which 10 µl was injected for LC-MS/MS analysis on an Ultimate 3000 RSLCnano system in-line connected to a Q Exactive HF mass spectrometer equipped with a Nanospray Flex Ion source (Thermo). Trapping was performed at 10 µl/min for 4 min in loading solvent A on a 20 mm trapping column (made in-house, 100 µm internal diameter (I.D.), 5 µm beads, C18 Reprosil-HD, Dr. Maisch, Germany) and the sample was loaded on a 400 mm analytical column (made in-house, 75 µm I.D., 1.9 µm beads C18 Reprosil-HD, Dr. Maisch). Peptides were eluted by a non-linear increase from 2 to 56% MS solvent B (0.1% FA in water/acetonitrile (2:8, v/v)) over 140 minutes at a constant flow rate of 250 nl/min, followed by a 15-minutes wash reaching 99% MS solvent B and re-equilibration with MS solvent A (0.1% FA in water/acetonitrile (2:8, v/v)). The column temperature was kept constant at 50°C in a column oven (CoControl 3.3.05, Sonation). The mass spectrometer was

operated in data-dependent mode, automatically switching between MS and MS/MS acquisition for the 16 most abundant ion peaks per MS spectrum. Full-scan MS spectra (375-1500 m/z) were acquired at a resolution of 60,000 in the orbitrap analyser after accumulation to a target value of 3,000,000. The 16 most intense ions above a threshold value of 13,000 were isolated (window of 1.5 Th) for fragmentation at a normalized collision energy of 32% after filling the trap at a target value of 100,000 for maximum 80 ms. MS/MS spectra (200-2000 m/z) were acquired at a resolution of 15,000 in the orbitrap analyser. The S-lens RF level was set at 55 and we excluded precursor ions with single and unassigned charge states from fragmentation selection.

Data analysis was performed with MaxQuant (version 1.5.3.30) using the Andromeda search engine with default search settings including a false discovery rate set at 1% on both the peptide and protein level. Spectra were searched against the mouse proteins in the UniProt/Swiss-Prot database (database release version of March 2016 containing 16,618 mouse protein sequences) with the mass tolerance for precursor and fragment ions set to 4.5 and 20 ppm, respectively, during the main search. Enzyme specificity was set as C-terminal to arginine and lysine (trypsin), also allowing cleavage at arginine/lysine-proline bonds with a maximum of two missed cleavages. Carbamidomethylation of cysteine residues was set as a fixed modification and variable modifications were set to oxidation of methionine residues (to sulfoxides) and acetylation of protein N-termini. Proteins were quantified by the MaxLFQ algorithm integrated in the MaxQuant software. Only proteins with at least one unique or razor peptide were retained for identification, while a minimum ratio count of two unique or razor peptides was required for quantification. Further data analysis was performed with the Perseus software (version 1.5.2.6) after loading the protein groups file from MaxQuant. Proteins were only identified by site, reverse database hits, and potential contaminants were removed and replicate samples were grouped. Proteins with less than three valid values in at

least one group were removed and missing values were imputed from a normal distribution around the detection limit. In this way, a total of 2,154 proteins were quantified.

The statistical analysis of the proteomic data was performed by an expert in biostatistics of the Proteomic Core Facility. A t-test, followed by permutation-based false discovery rate estimation (1000 permutations) was performed (FDR=0.05 and S0=0.5) to reveal proteins that are significantly different between WT and *Parl*$^{-/-}$ samples and to generate the volcano plot depicted in Fig.6*A*.

Plasmids

All mouse *Parl* mutants were constructed using the QuickChange II XL mutagenesis kit (Stratagene). Immortalized mouse embryonic fibroblasts (MEFs) derived from *Parl*$^{-/-}$ mice were cultured in Dulbecco's modified Eagle's medium/F-12 (Gibco) containing 10% fetal bovine serum (Gibco). At 30–40% confluence, the MEFs were transduced using a replication-defective recombinant retroviral expression system (Clontech) with either wild-type (*Parl*^{WT}) or with catalytic inactive *Parl*^{S275A}. Cell lines stably expressing the desired proteins were selected based on their acquired resistance to 5 µg/ml puromycin.

Evaluation of Cre mediated recombination in peripheral tissues of the *Parl*$^{L/L}$*::Nes*^{Cre} mouse

Genomic DNA was isolated using DNeasy Blood and Tissue Kit (Qiagen) according to the manufacturers guidelines, PCR was performed using KAPA Mouse Genotyping Kit (KAPA Biosystems) and samples were analysed on the QIAXcel Advanced System (Qiagen)

Primer sequences were:

Parl conditional allele P3 = AGCACCCAGGAAGGTTGAACCT; P2 = TGTGGCCGTATGCTGTCCACC

internal control *Mapt:* F = CGCCAGGAGTTCGAAGTGA; R = CTAGGCCACAGAATTGAAAGATCT

Parl KO allele: P1 = CTTAATAGGGAATGGGAGTTGCAC; P2 = TGTGGCCGTATGCTGTCCACC

Equal amount of input DNA was used and cycle numbers were in the exponential range of the PCR (for the WT allele 27 cycles for liver and spleen, 30 cycles for muscle, 32 cycles for thymus; for the KO allele 32 cycles for all organs).

mtDNA quantification

Isolation of DNA was done using the Qiagen Dneasy Blood and Tissue kit following the manufacturers instructions. Real-time semi-quantitative PCR was performed on a LightCycler 480 (Roche) using the SensiFast Sybr No ROX Mix (Bioline) according to the manufacturers instructions. In each reaction 1,5ng of gDNA was used. Sequences of the primers used can be found in the table below. Crossing points were determined by using the second derivative method. Fold changes were calculated with the ΔΔCt method (18).

mt-Co1 forward	TCGCCATCATATTCGTAGGAG
mt-Co1 reverse	GTAGCGTCGTGGTATTCCTGA
mt-Nd4 forward	TTATTACCCGATGAGGGAACC
mt-Nd4 reverse	GAGGGCAATTAGCAGTGGAAT
Apob forward	CGTGGGCTCCAGCATTCTA
Apob reverse	TCACCAGTCATTTCTGCCTTT
B2m forward	TGTCAGATATGTCCTTCAGCAAGG
B2m reverse	TGCTTAACTCTGCAGGCGTATG

Cell culture

Mouse primary neurons were cultured using a protocol adapted from Goslin and Banker (19). Briefly, E14,5 mouse whole brains were trypsinized, dissociated with fire-polished Pasteur pipets, and plated onto poly-L-lysine (Sigma)-coated culture dishes. Cells were incubated for the first 4 h in minimum essential medium (MEM) with 10% horse serum and then

maintained in serum-free neurobasal medium with B27 supplement (Gibco). All cells were incubated at 37°C with 5% CO2. When specified, after one week in culture, neurons were treated with 10µM etoposide for 24h before collection.

Statistical analysis

All numerical data are expressed as mean ± SD. Two sided student's t test was used to compare differences between two groups and ANOVA was used to compare differences between multiple groups and to correct results for multiple comparisons using GraphPad 7. Statistical significance for survival curves was calculated by log-rank (Mantel-Cox). Differences were considered statistical significant for $p \leq 0.05$. Mass spectrometry data were analyzed by a specialist in biostatistics (T.M.) as detailed in the LC-MS/MS and data analysis section.

Data availability

The mass spectrometry proteomics data have been deposited to the ProteomeXchange Consortium via the PRIDE (20) partner repository with the dataset identifier PXD008908.

REFERENCES

1. Cipolat S, et al. (2006) Mitochondrial Rhomboid PARL Regulates Cytochrome c Release during Apoptosis via OPA1-Dependent Cristae Remodeling. *Cell* 126(1):163–175.
2. Tronche F, et al. (1999) Disruption of the glucocorticoid receptor gene in the nervous system results in reduced anxiety. *Nat Genet* 23(1):99–103.
3. Brüning JC, et al. (1998) A muscle-specific insulin receptor knockout exhibits features of the metabolic syndrome of NIDDM without altering glucose tolerance. *Mol Cell* 2(5):559–69.
4. Morais VA, et al. (2009) Parkinson's disease mutations in PINK1 result in decreased Complex I activity and deficient synaptic function. *EMBO Mol Med* 1(2):99–111.
5. Kaufmann W, et al. (2012) Proliferative and Nonproliferative Lesions of the Rat and Mouse Central and Peripheral Nervous Systems. *Toxicol Pathol* 40(4_suppl):87S–157S.
6. Seuntjens E, et al. (2009) Sip1 regulates sequential fate decisions by feedback signaling

from postmitotic neurons to progenitors. *Nat Neurosci* 12(11):1373–1380.

7. Sims NR, Anderson MF (2008) Isolation of mitochondria from rat brain using Percoll density gradient centrifugation. *Nat Protoc* 3(7):1228–1239.

8. Jha P, Wang X, Auwerx J (2016) Analysis of Mitochondrial Respiratory Chain Supercomplexes Using Blue Native Polyacrylamide Gel Electrophoresis (BN-PAGE). *Curr Protoc Mouse Biol* 6(1):1–14.

9. Fasching M, Renner-sattler K, Gnaiger E (2016) Mitochondrial Respiration Medium - MiR06. *Mitochondrial Physiol Netw* 14.13(6):1–4.

10. Spinazzi M, Casarin A, Pertegato V, Salviati L, Angelini C (2012) Assessment of mitochondrial respiratory chain enzymatic activities on tissues and cultured cells. TL - 7. *Nat Protoc* 7(6):1235–1246.

11. Spinazzi M, et al. (2011) Optimization of respiratory chain enzymatic assays in muscle for the diagnosis of mitochondrial disorders. *Mitochondrion* 11(6):893–904.

12. Rodríguez-Aguilera J, Cortés A, Fernández-Ayala D, Navas P (2017) Biochemical Assessment of Coenzyme Q10 Deficiency. *J Clin Med* 6(3):27.

13. Starkov AA Measurement of Mitochondrial ROS Production. 648:16–23.

14. Krumschnabel, G., Fontana-Ayoub, M., Sumbalova, Z., Heidler, J., Gauper K, Fasching, M., and Gnaiger E (2015) Simultaneous high-resolution measurement of mitochondrial respiration and hydrogen peroxide production. *Methods Mol Biol* 1264:245–261.

15. Wang P, Powell SR (2010) Decreased sensitivity associated with an altered formulation of a commercially available kit for detection of protein carbonyls. *Free Radic Biol Med* 49(2):119–121.

16. Panov A, et al. (2009) The neuromediator glutamate, through specific substrate interactions, enhances mitochondrial ATP production and reactive oxygen species generation in nonsynaptic brain mitochondria. *J Biol Chem* 284(21):14448–14456.

17. Krumschnabel G, Eigentler A, Fasching M, Gnaiger E (2014) *Use of safranin for the assessment of mitochondrial membrane potential by high-resolution respirometry and fluorometry* (Elsevier Inc.). 1st Ed. doi:10.1016/B978-0-12-416618-9.00009-1.

18. Livak KJ, Schmittgen TD (2001) Analysis of relative gene expression data using real-time quantitative PCR and the 2-ΔΔCT method. *Methods* 25(4):402–408.

19. Goslin K, Banker G (1990) Rapid changes in the distribution of GAP-43 correlate with the expression of neuronal polarity during normal development and under experimental conditions. *JCell Biol* 110(4):1319–1331.

20. Vizcaíno JA, et al. (2016) 2016 update of the PRIDE database and its related tools. *Nucleic Acids Res* 44(D1):D447–D456.

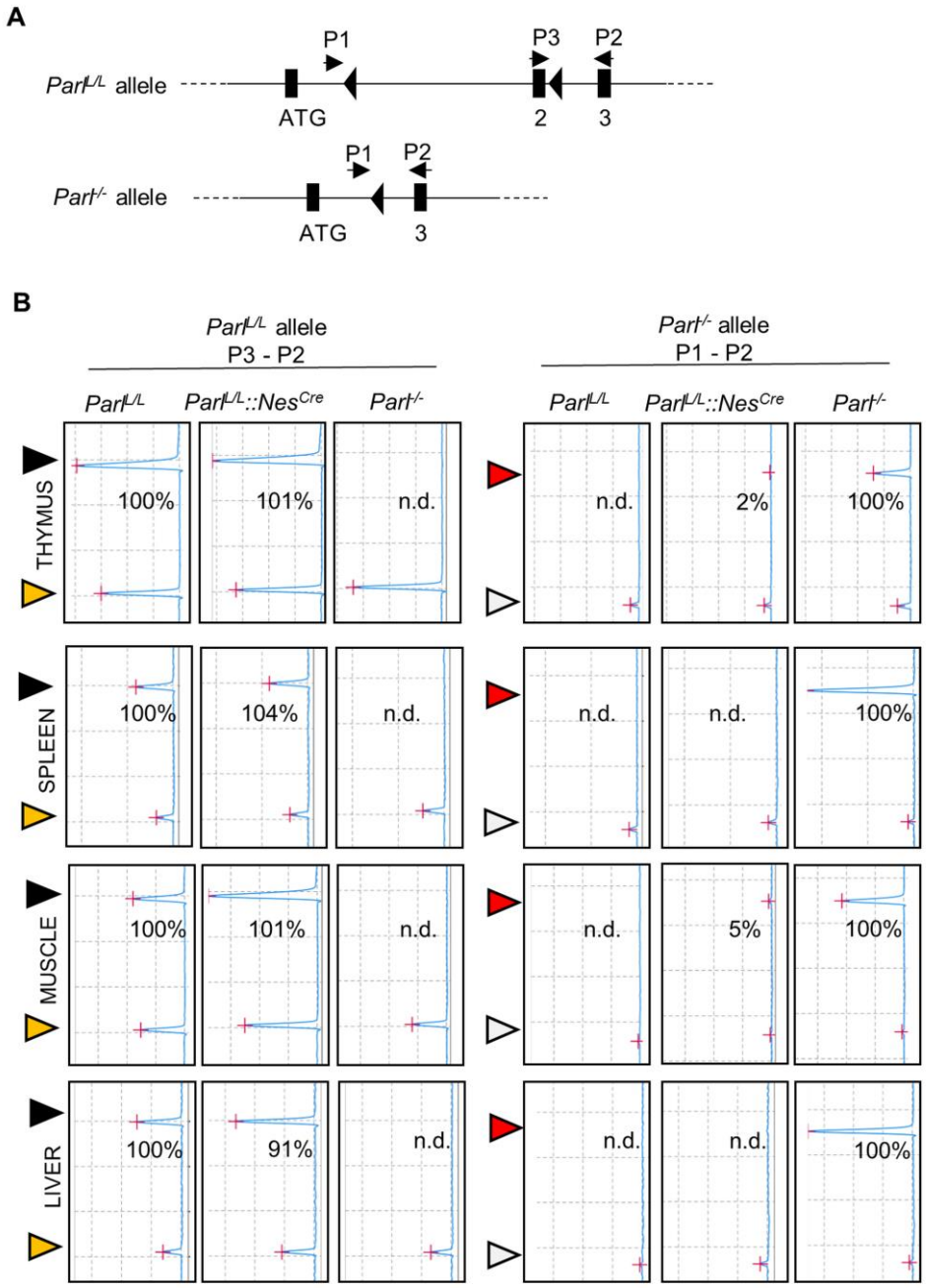

Fig. S1

Evaluation of *Cre* mediated recombination in peripheral tissues of the *Parl*$^{L/L}$*::Nes*^{Cre} mouse.
(*A*) Schematic representation of the PCR strategy used to amplify *Parl*$^{L/L}$ and *Parl*$^{-/-}$ alleles in tissues from 7 weeks-old WT (*Parl*$^{L/L}$) and *Parl*$^{-/-}$ and 12 weeks-old *Parl*$^{L/L}$*::Nes*^{Cre}. (*B*) PCR reactions were stopped before linear phase of the amplification and products were analyzed by high-resolution capillary electrophoresis (QIAXcel Advanced System). The black arrow indicates the allele-specific signal for *Parl*$^{L/L}$, the orange arrow indicates the internal control signal for *Mapt*. The red arrow indicates the *Parl*$^{-/-}$ specific signal. An aspecific signal indicated by grey arrow is used as internal control for *Parl*$^{-/-}$ PCR. The quantifications are normalized to the internal control products. n.d. = non detectable (n=3 for spleen, muscle, liver, n=2 for thymus).

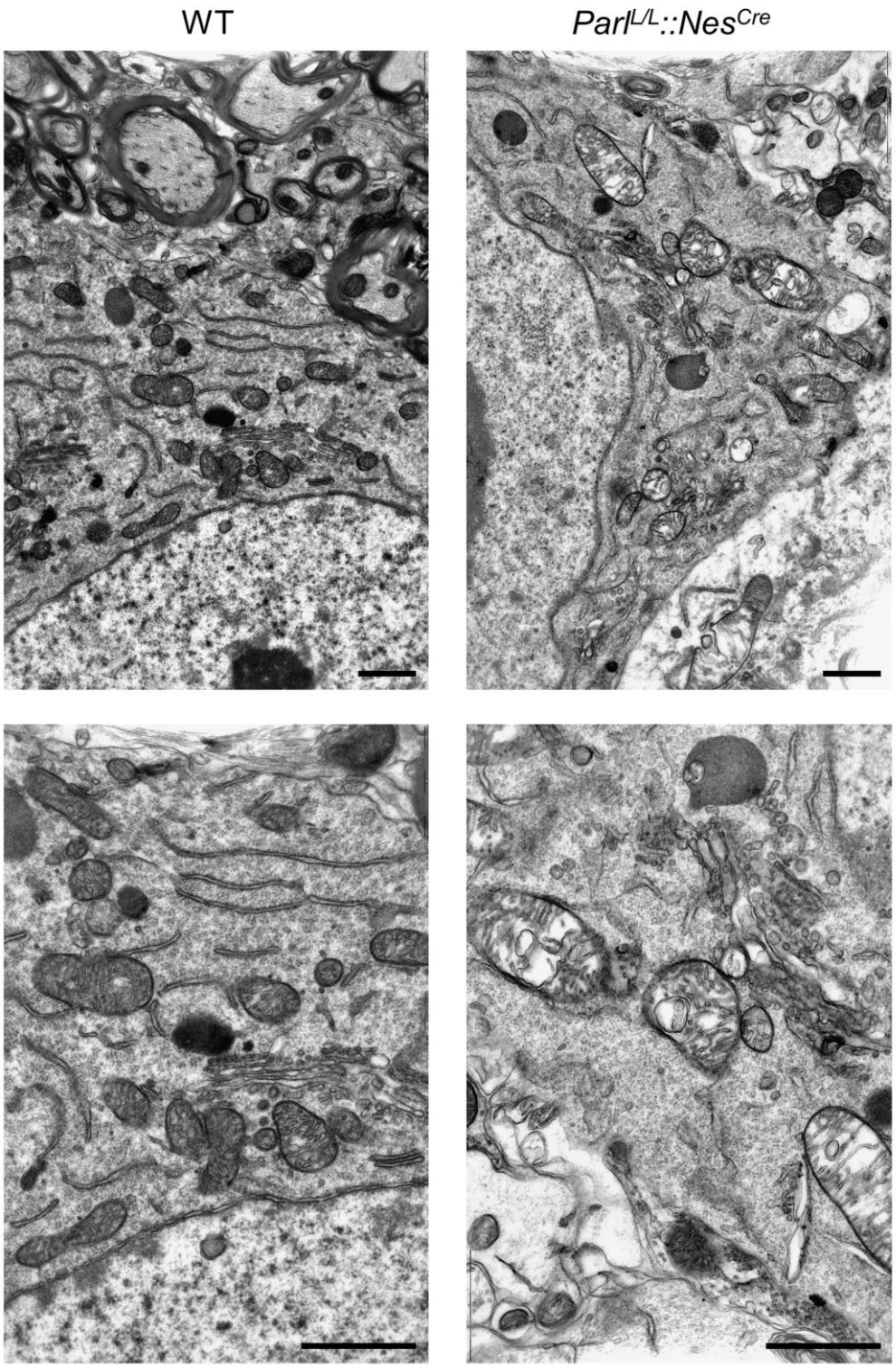

Fig. S2

Mitochondrial ultrastructural abnormalities in *Parl*$^{L/L}$*::Nes*^{Cre} brainstem mitochondria. Representative transmission electron micrograph showing several mitochondria with severely altered ultrastructure in neurons of medulla oblongata from 5 weeks old *Parl*$^{L/L}$*::Nes*^{Cre}, but not in WT.Scalebar:1µm.

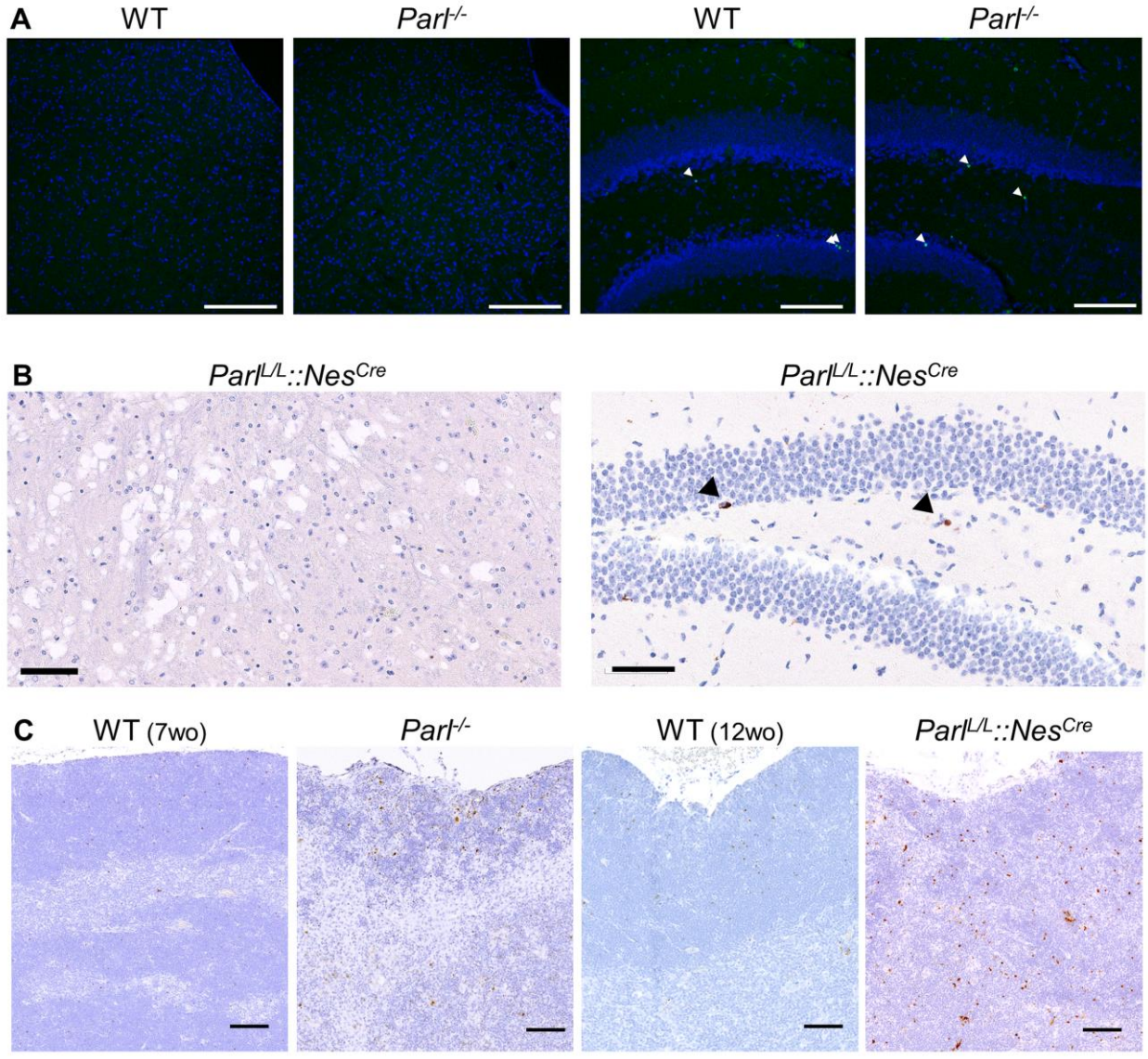

Fig. S3

Execution of apoptosis is unaffected in PARL deficient brains and indirectly increased by PARL deficiency in thymus. (*A*) TUNEL/DAPI staining shows absence of TUNEL positive neurons in six weeks old WT and *Parl*$^{-/-}$ medulla oblongata (left; scale bar: 200 µm), and scattered positive neurons in hippocampus (white arrows in the right panel; scale bar 100 µm). (*B*) Activated-CASP3 staining shows absence of positive neurons in 3 months old *Parl*$^{L/L}$*::Nes*^{Cre} thalamus (left) despite the presence of severe neurodegeneration. Scale bar: 80 µm. In the neurogenic region of the dentate gyrus (right), a brain area that has never presented neurodegeneration in the germline and in the *Parl*$^{L/L}$*::Nes*^{Cre}, activated-CASP3 staining shows scattered positive neurons (black arrows) as shown in Fig 2*H* also in WT and *Parl*$^{-/-}$. Scale bar: 25 µm. (*C*) Strong increase in anti-activated-caspase3 staining in atrophic thymus from a seven week-old *Parl*$^{-/-}$ mice and a 12 weeks-old *Parl*$^{L/L}$*::Nes*^{Cre} compared to age matched WT. Scale bar:100 µm.

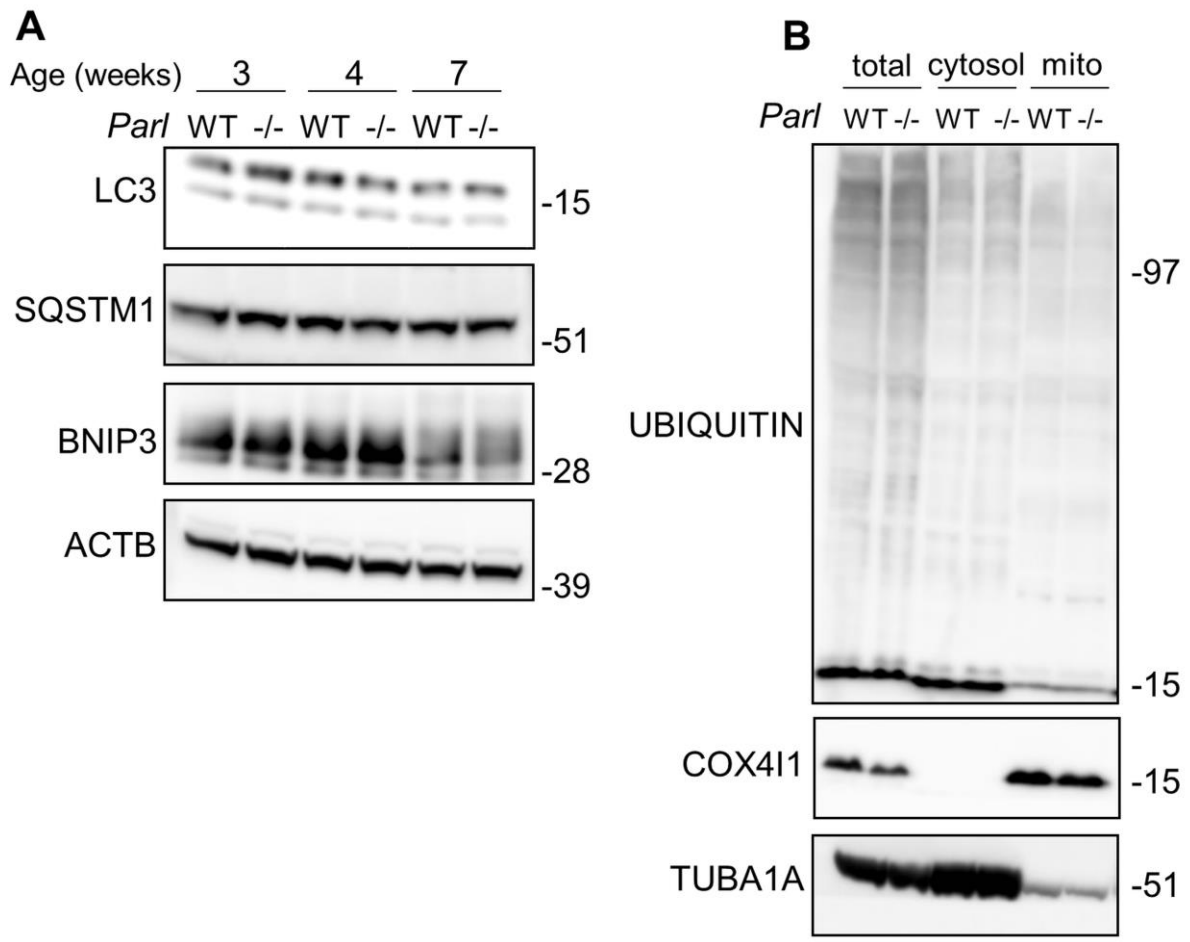

Fig. S4

Unaltered markers of autophagy and mitochondrial protein ubiquitination in *Parl*$^{-/-}$ brains.
(*A*) Total lysates from WT and *Parl*$^{-/-}$ brains were prepared at the indicated time points and run through SDS-page, and immunoblotted for different autophagy markers LC3, SQSTM1, BNIP3. ACTB is the loading control. (*B*) Six week-old brains from WT and *Parl*$^{-/-}$ mouse were homogenized and further sub-fractionated into the cytosolic and mitochondrial fractions. Brain total homogenates, cytosol and purified mitochondria were analyzed by SDS-page and immunoblotting using anti-Ubiquitin antibody. COX4I1 is the mitochondrial marker, TUBA1A is the cytosolic marker.

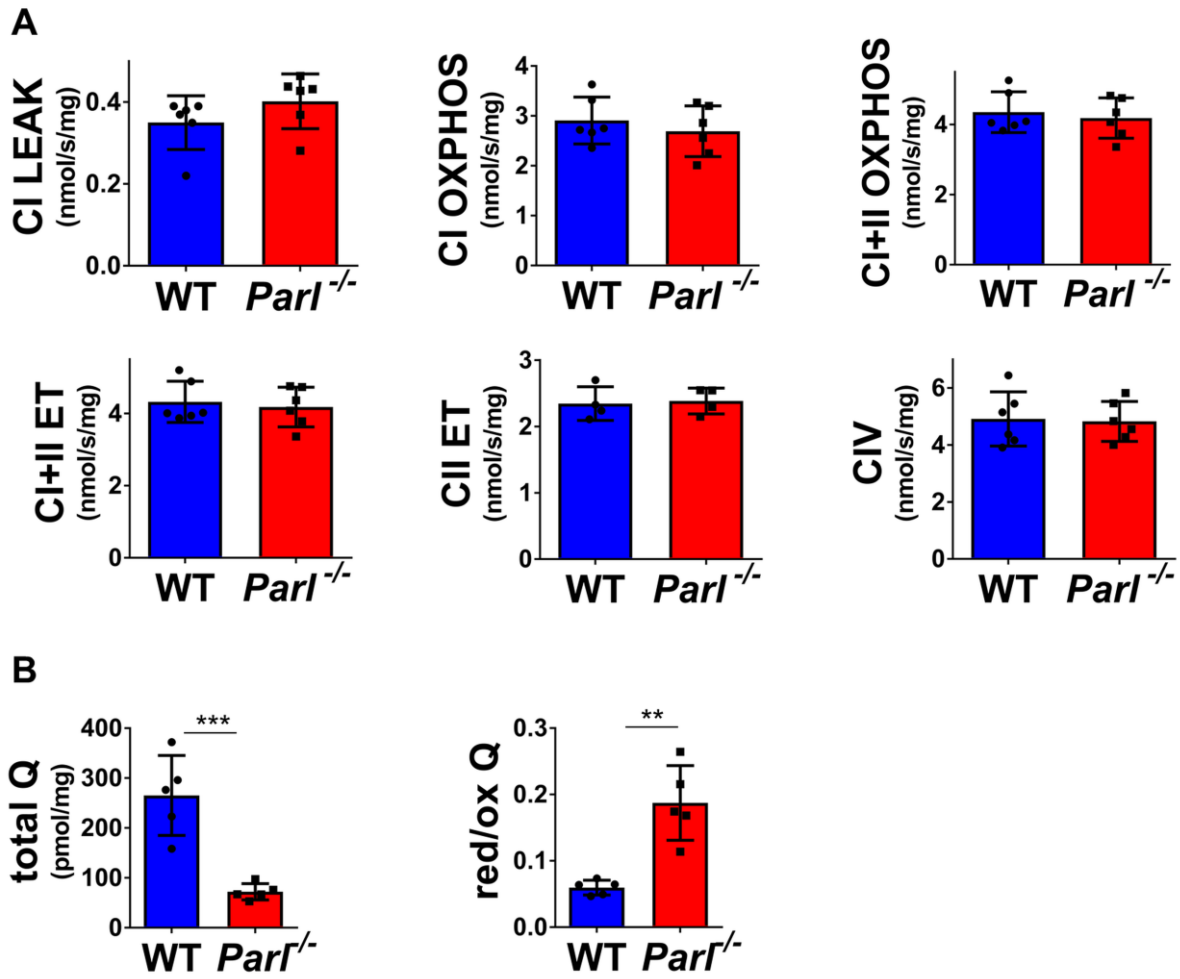

Fig. S5

Mitochondrial neuronal respiration and CoQ in brains of presymptomatic *Parl*$^{-/-}$ mice. (*A*) High resolution respirometry of synaptosomal mitochondria derived from three-weeks old WT and *Parl*$^{-/-}$ mice (n=6 for each genotype). No respiratory state reached statistical significance by two sided student t test. (*B*) Concentration (left) and red/ox ratio (right) of total coenzyme Q (Q_9 and Q_{10}) measured by HPLC in brain tissue from three weeks old WT and *Parl*$^{-/-}$ mice (n=5 for each genotype). The bar graphs indicate the average ± SD. Statistical significance has been calculated by two sided student-t test. **=p<0,01; ***=p<0,001.

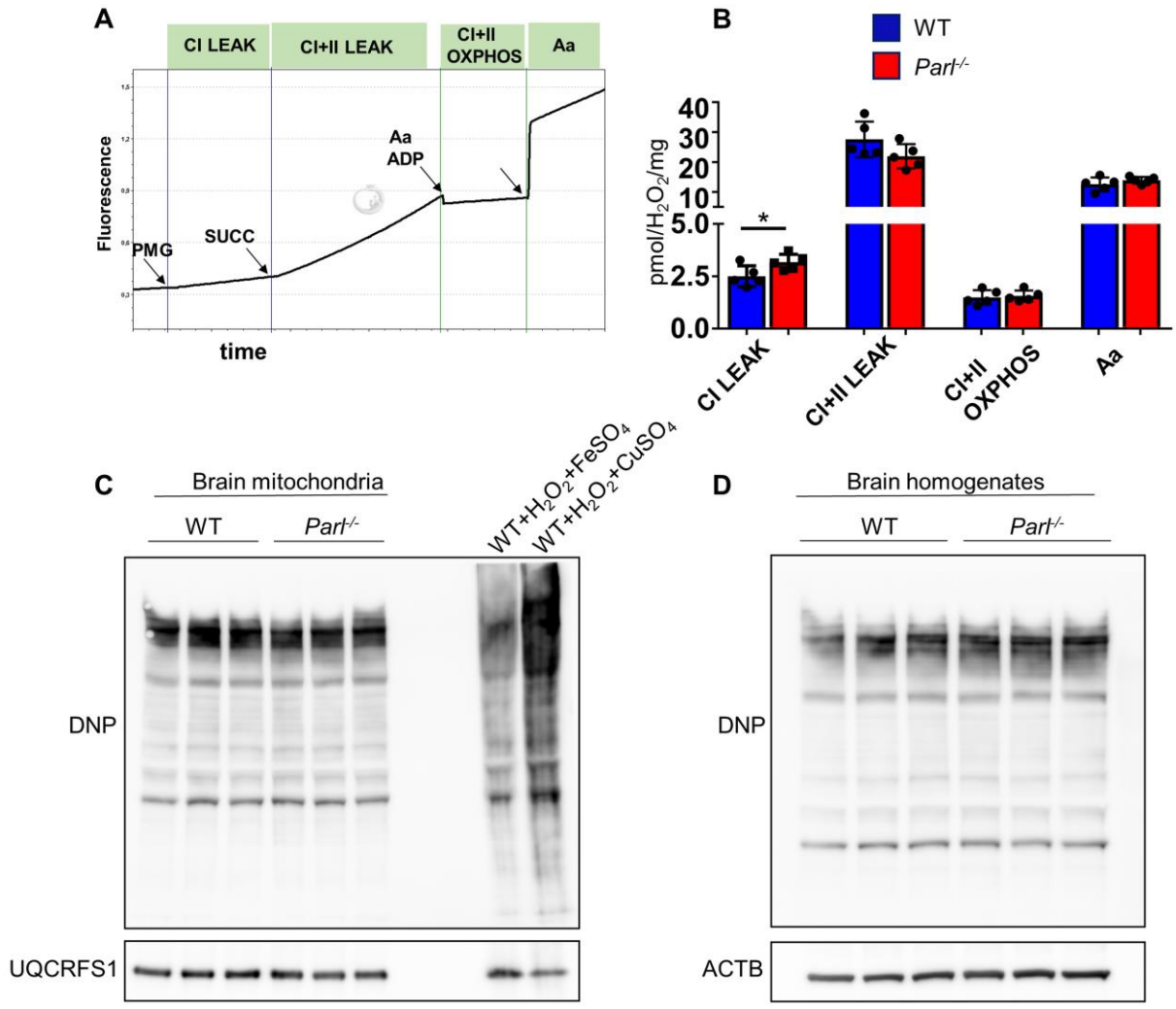

Fig. S6

ROS production and oxidative stress in *Parl*$^{-/-}$ brains. (*A*) Representative trace illustrating the protocol for measuring ROS production by fluorometry in brain mitochondria. 150 µg brain mitochondria were loaded in the O2k chamber equipped with a fluorometry module at 37 C with 10µM Amplex Ultrared as described in the methods section. The fluorescence intensity is calibrated for each run with H_2O_2 standards in presence of superoxide dismutase. Substrates: Complex I (PMG=pyruvate+malate+glutamate), Complex II (Succ=succinate). ROS production is first measured in absence of ADP, a condition that leads to high membrane potential and stimulate ROS production initially with only Complex I substrates (CI Leak), and then also with the Complex II substrate succinate (CI+II Leak). After addition of ADP H_2O_2 production is measured in phosphorylating conditions (CI+II OXPHOS). In this experimental condition, the greatly decreased H_2O_2 production rate reflects the decreased mitochondrial potential. Finally Antimycin a, a specific Complex III inhibitor, is added to measure H_2O_2 production from this complex. (*B*) Quantifications of the experiments described in A with brain mitochondria from 7 weeks old WT and *Parl*$^{-/-}$ mice (n=5). The graph bars indicate the mean ± SD. Statistical significance has been calculated by two sided t-test: *= p<0,05. (*C*) Protein carbonylation in 7 weeks old WT and *Parl*$^{-/-}$ brain mitochondria by using anti DNP immunoblot (n=3). UQCRFS1 is the loading control. WT brain mitochondria treated with H_2O_2+$FeSO_4$ and H_2O_2+$CuSO_4$ were included as positive controls. (D) Protein carbonylation in 7 weeks old WT and *Parl*$^{-/-}$ brain homogenates (n=3). ACTB is the loading control.

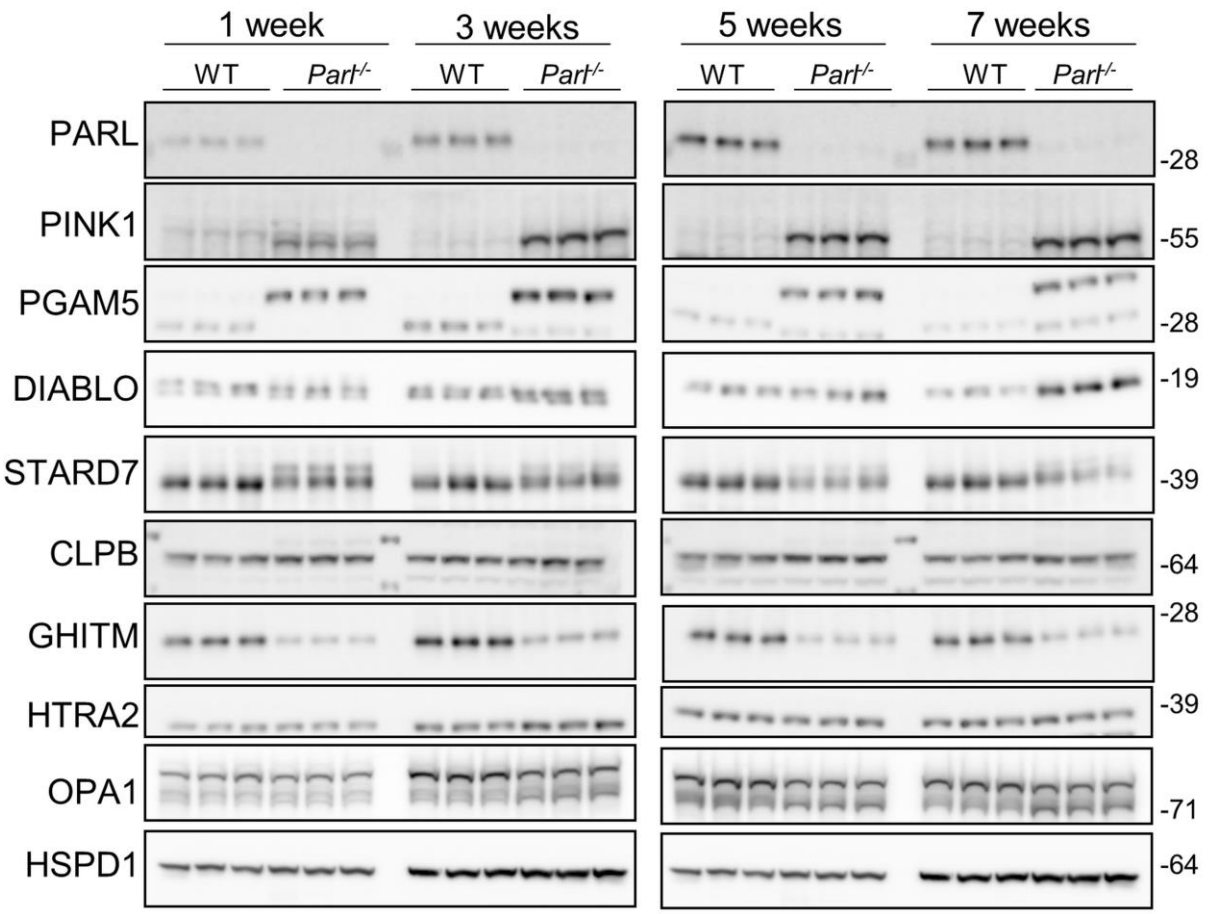

Fig. S7

Time course of protein changes within time in *Parl*$^{-/-}$ brains. 20 µg of total brain lysates from WT and *Parl*$^{-/-}$ mice sacrificed at 1, 3, 5, and 7 weeks of age (n=3 for each genotype for each time point), were analyzed by SDS page followed by immunoblotting with the indicated antibodies. Unprocessed forms of PGAM5 and STARD7 are visible in *Parl*$^{-/-}$ samples. HSPD1 is the loading control.

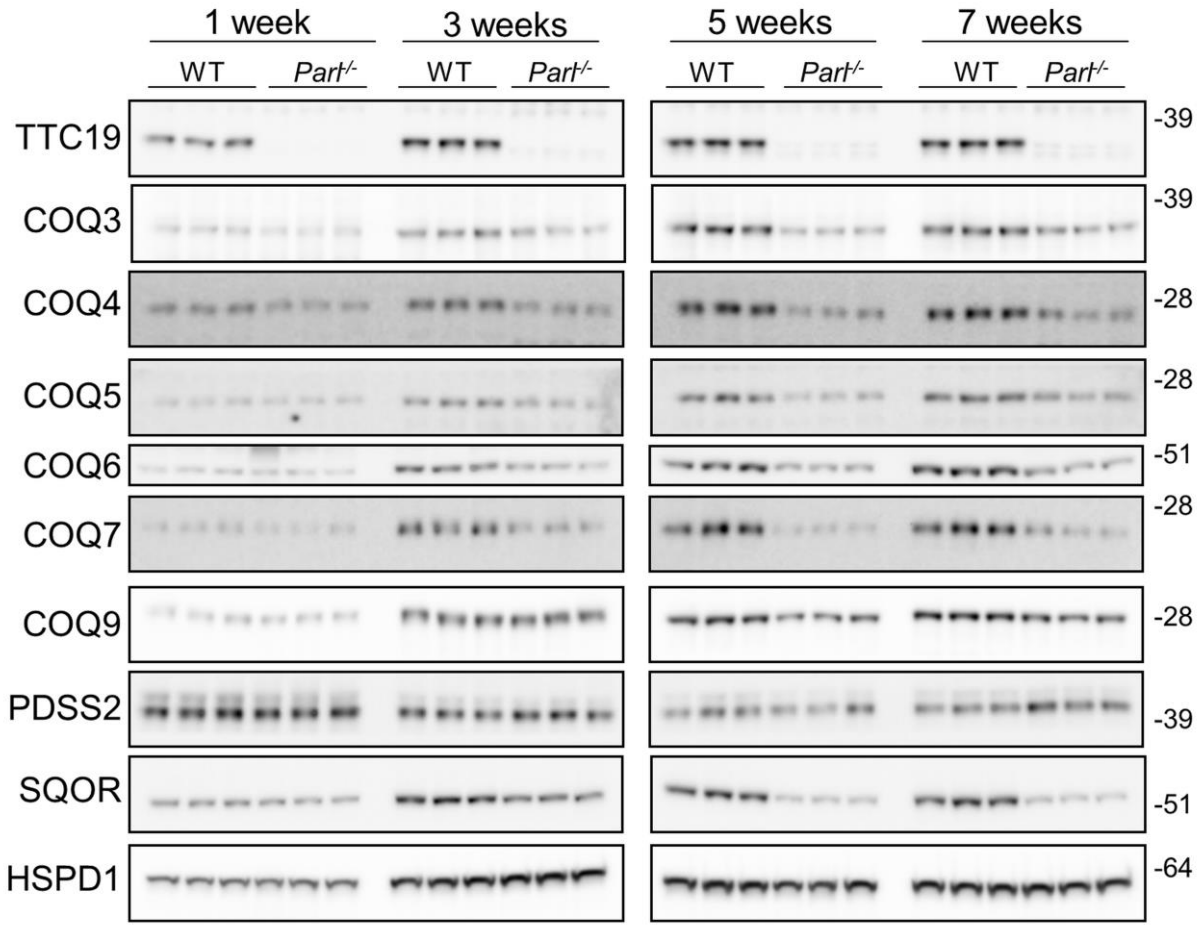

Fig. S8

Expression within time of TTC19 and CoQ-related proteins in *Parl*$^{-/-}$ brains. Western blot used for the quantifications illustrated in Fig.6C. 20 µg of total brain lysates from WT, *Parl*$^{-/-}$ sacrificed at 1, 3, 5, and 7 weeks of age (n=3 for each genotype for each time point), were analyzed by SDS page followed by immunoblotting with the indicated antibodies. HSPD1 is the loading control.

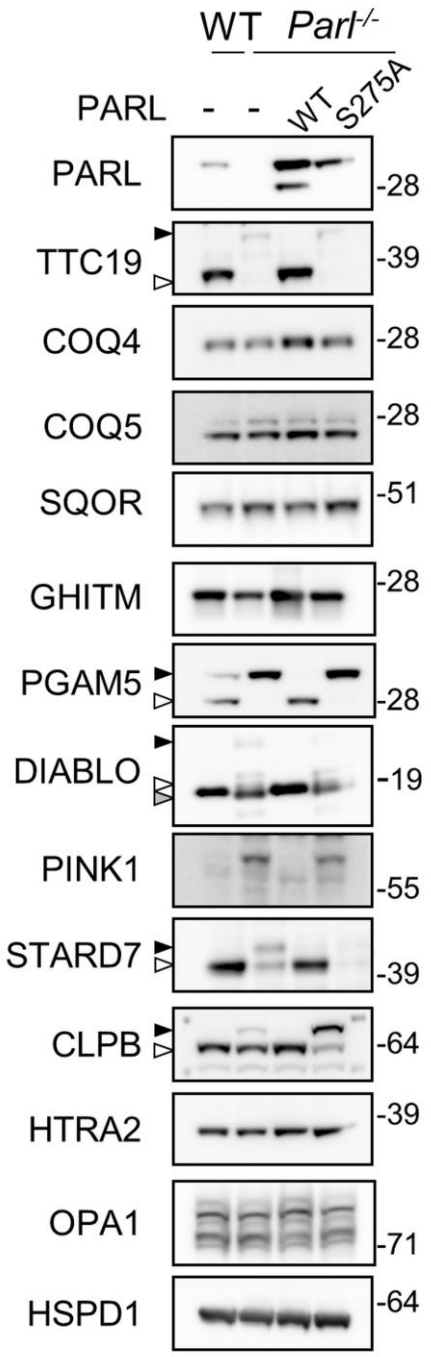

Fig S9

Effect of PARL proteolytic activity in mouse embryonic fibroblasts on proteins differentially regulated by PARL. 20 µg of mitochondria isolated from WT and *Parl*$^{-/-}$ MEFs complemented or not with WT or catalytic inactive PARLS275A were separated by SDS page and immunoblotted with the indicated antibodies. One representative experiment is shown from three independent experiments. The white arrows indicate the mature processed form of the protein, the black arrows unprocessed forms of the protein, the grey arrows indicate alternatively processed forms of the proteins in *Parl*$^{-/-}$ mitochondria. HSPD1 is the loading control.

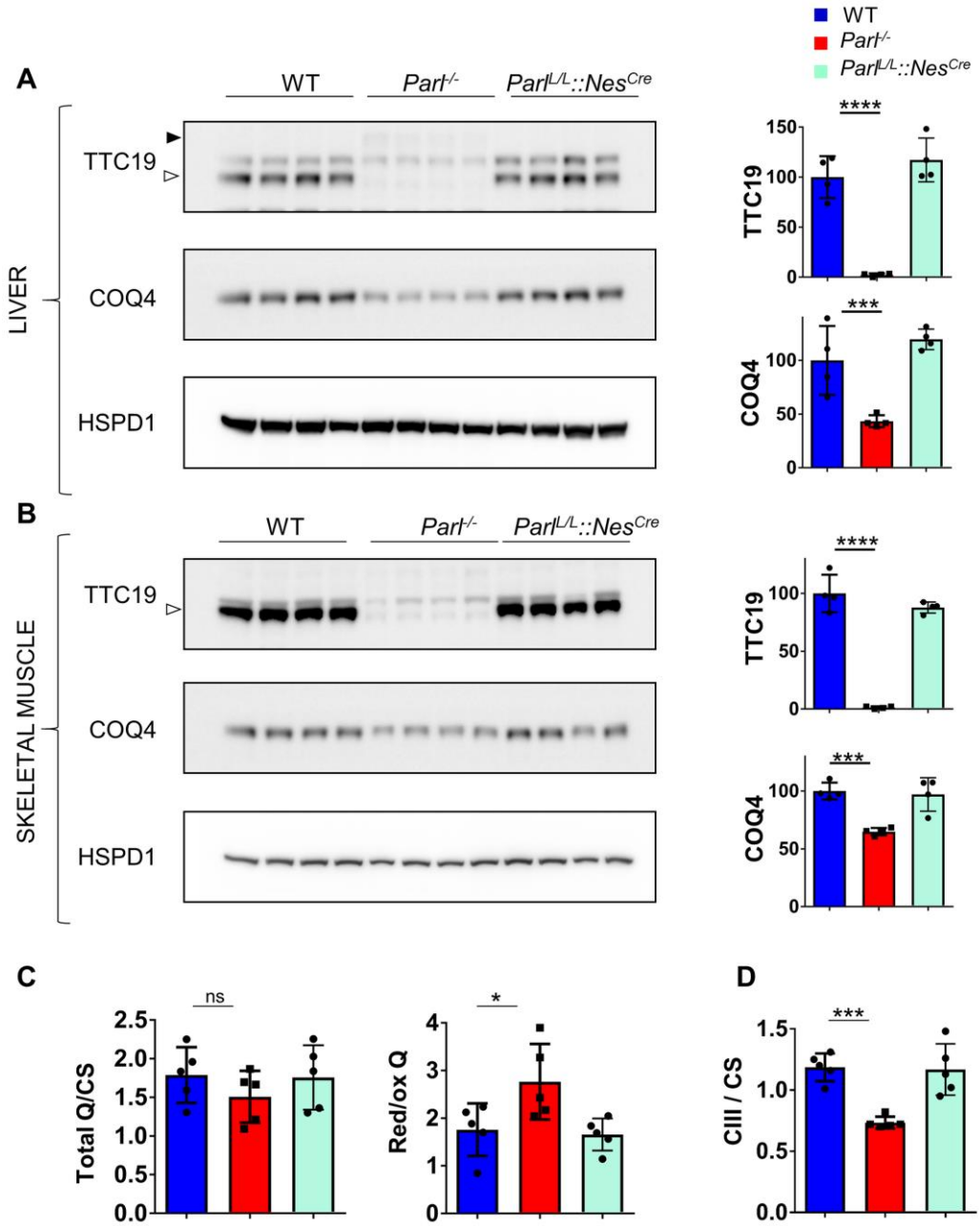

Fig. S10

Effect of PARL deficiency on Complex III and CoQ in liver and muscle. (*A-B*) Expression of TTC19 and COQ4 in WT, *Parl*$^{-/-}$, and *Parl*$^{L/L}$*::Nes*^{Cre} (n=3 for each genotype) at 7 weeks of age in liver (*A*) and gastrocnemius skeletal muscles (*B*). The white arrow indicates TTC19 specific band and the black arrow indicates the unprocessed form of TTC19. 20 µg of total lysates were analyzed by SDS page followed by immunoblotting. The graph bars indicate the quantifications of the western blot results, normalized with the loading control HSPD1 and expressed as % relative to the WT. (*C*) Concentration of total CoQ (Q_9+Q_{10}) normalized to citrate synthase activity and ratio between reduced and oxidized CoQ in gastrocnemius skeletal muscles from WT, *Parl*$^{-/-}$, and *Parl*$^{L/L}$*::Nes*^{Cre} at 7 weeks of age measured by HPLC (n=5 for each genotype). (*D*) Complex III enzymatic activity normalized by citrate synthase activity in skeletal muscle homogenates from gastrocnemius muscles of WT, *Parl*$^{-/-}$, and *Parl*$^{L/L}$*::Nes*^{Cre} at 7 weeks of age. The graph bars indicate the mean ± SD. Statistical significance has been calculated by ANOVA and corrected for multiple comparisons: *= p<0,05; ***=p<0,001;****=p<0,0001.

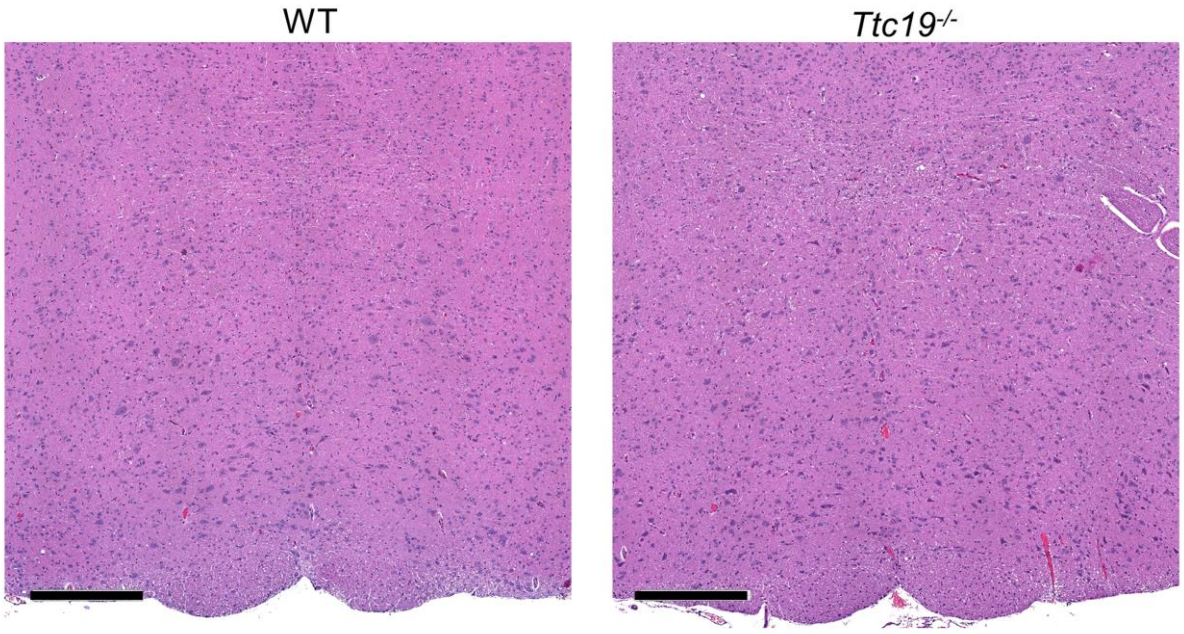

Figure S11

Neuropathological analysis of *Ttc19*$^{-/-}$ mice. Representative H&E staining of the medulla oblongata of 7-week old *Ttc19*$^{-/-}$ and WT mouse showing absence of neurodegeneration (n=3). Scale bar: 200 µm.

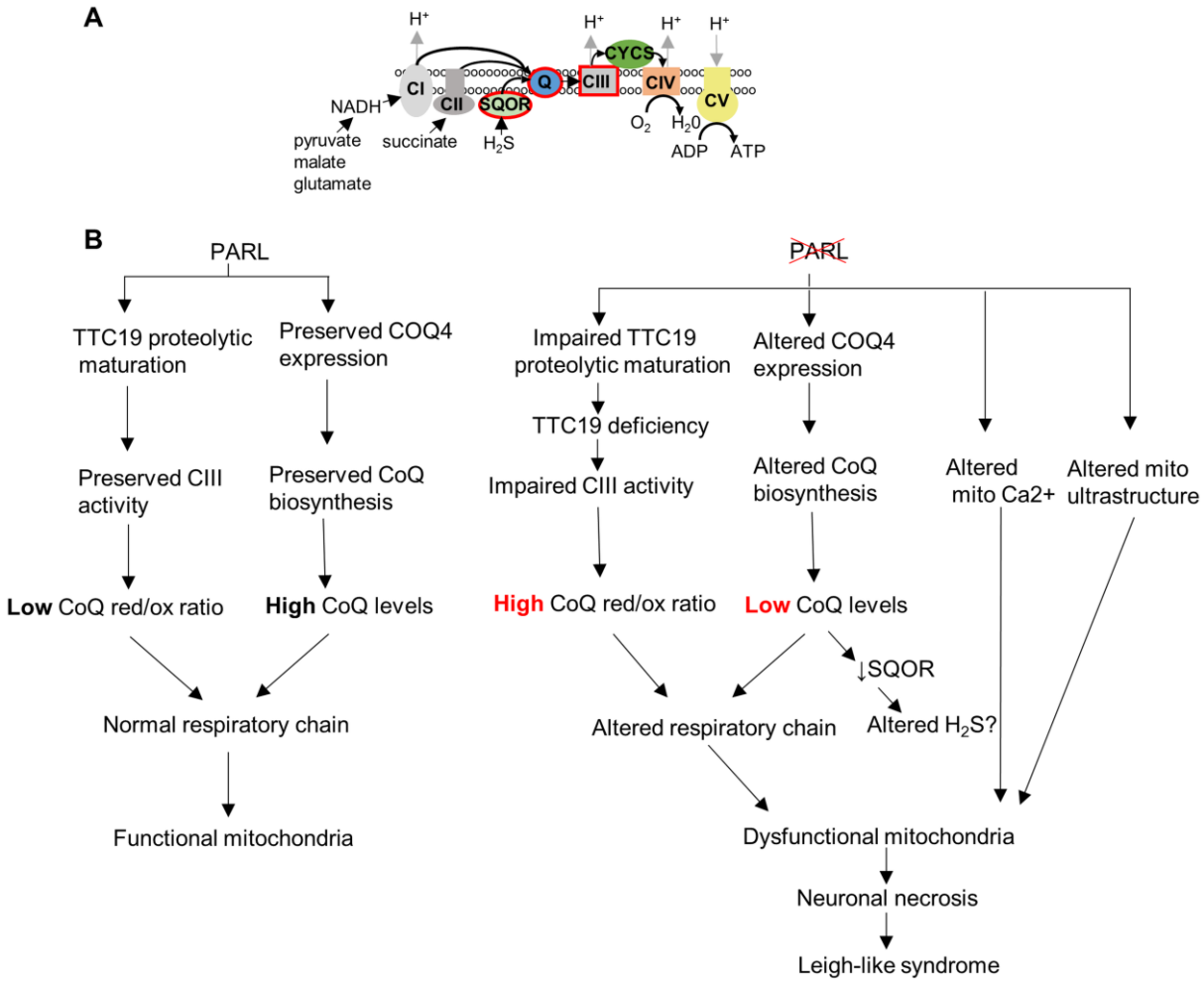

Fig. S12

Schematic illustration of the role of PARL in mitochondrial respiratory chain homeostasis. (*A*) Cartoon illustrating the mitochondrial respiratory chain. CI: Complex I; CII: Complex II; CIII: Complex III; CIV: Complex IV; CV: ATP synthase; SQOR:sulfide quinone oxidoreductase; Q: Coenzyme Q; CYCS: cytochrome c. The sites encircled in red are affected by PARL deficiency. Coenzyme Q, a lipophilic quinone embedded in the inner mitochondrial membrane, constitutes an electron transfer chain relay site, receiving electrons from Complex I (derived from NADH oxidation), from complex II (derived from succinate oxidation), from SQOR (derived from sulfide oxidation) and from other metabolic enzymes. Electrons are then transferred from reduced coenzyme Q to cytochrome c by complex III, then from cytochrome c to molecular oxygen by complex IV. (*B*) Schematic diagram illustrating how Parl expression affects the respiratory chain function in the nervous system. PARL deficiency in neuronal mitochondria leads also to altered mitochondrial calcium metabolism and progressive ultrastructural abnormalities that might also contribute to the Leigh-like necrotizing encephalopathy.

Table S1. Proteins quantified by mass spectrometry.

Proteins quantified by quantitative label free mass spectrometry of brain mitochondria. purified from 5 week-old WT and *Parl*$^{-/-}$ mouse brains (n=3 for each group).

Movie S1. Locomotor impairment of *Parl*$^{-/-}$ mouse. Two seven week-old *Parl*$^{-/-}$ mice show the typical locomotor impairment, severe muscle atrophy, and dyspnea, at difference with an age matched WT littermate.